

Heat Temperature Effect on Land-use and Land-cover Dynamics using Geospatial Techniques from Normalize Build-up Index (NDBI), Land Surface Temperature (LST) and Normalize Vegetation Index (NDVI)

Aminu Abdulwahab ^a, Danladi Drambi ^b

a Department of Surveying and Geoinformatics, Federal Polytechnic Mubi PMB 35, Mubi Adamawa State Nigeria.

b Department of Urban and Regional Planning, Federal Polytechnic Mubi PMB 35, Mubi Adamawa State Nigeria.

Corresponding Author: Aminu Abdulwahab

Abstract

This research attempt to explore the geospatial technology to Model the spatiotemporal pattern and the impact of the normalised Build-up index (NDBI), the L S T and NDVI, and how it influences the land use/ land cover (LU/LC) of the region under study. The project depicts the dynamics of urban heat island (UHI) and how they impact the (LU/LC) for 4 epochs (2004 to 2019). We have also detected and identify the dynamics variation in land cover changes that occurred during 15 years leveraging both open/license source software such as R and GEE, ArcGIS 10.6, Envi 5.3 and. The multi-temporal Landsat satellites images (ETM, and ETM+) covering the Mubi region 2004, 2009, 2014 and 2019 were used as the primary data sources for this project. The global mapper 19 software, Google Earth Pro, <https://earthexplorer.usgs.gov/> & <http://glovis.usgs.gov>, were used for image acquisition while the ArcGIS 10.6, Erdas Imagine 2015 and R software were used in the data analysis. From the analysis, the urban area has expanded by 1437.26 Hectares (27.34%) and vegetated land was reduced by 425.82 Hectares (-8.08%), the water body reduced by 142.24 hectares (2.70%), fallow land reduces by 701.888 hectares (-13.32%), open land also reduced by 3.491 hectares (-0.04%) and the rock land was also reduced by 168.11 hectares (-3.19%) from the period of this project we observe that all the land uses lost their sizes except the urban area which increases by a large percentage. The mean land surface temperature (LST) for 2004 was 15.59°C then it increases to 20.16°C in 2009 it further increases to 20.74°C and finally 24.88°C the mean increase for epoch was observed as a result of urban area growth as demonstrated from the R statistical analyses of this project. A lower negative correlation was experienced when comparing the LST and the NDVI by selecting 32 random spatial locations of the vegetation land (VL) within the Mubi region. similarly, a higher positive correlation was experienced when comparing the LST with NDBI for the four epochs from 2004-2019. The magnitude of mean LST was calculated based on the main LU/LC categories, where urban land (UL) recorded the higher temperature difference compared to open land (OL) and water bodies (WB). However, the vegetation land (VL) recorded the lowest mean LST differences within all the other LU/LC categories. In addition to that, there was an overall negative correlation between LST and the normalized difference vegetation index (NDVI). There was an overall positive correlation between LST and the normal difference built-up index (NDBI).

Keywords: *LST, LU/LC, Spatiotemporal, Landsat, Regression analysis, NDVI, Geospatial model*

Date of Submission: 13-07-2021

Date of Acceptance: 29-07-2021

I. Introduction

Research has shown that the LU/LC has experienced a rapid change over time due to human activities on it. Some of the changes are influenced by many factors such as cultural, agricultural, political, historical and economic at large scale (Abdulwahab A. et al, 2019). On a Globally level, the urban population has increased to 54.5% (in 2016), the persistence in these trends will hence lead to urban population growth to 60% of the global total in 2030 (The

World's Cities In 2016). The fast change through rapid development in the area of land use/land spread (LU/LC) has impacts on the lower scale environment and the variables within the surrounding climate and the perspective of its economy (Wang, R. et al. 2018). (Singh, P et al. 2017) express that the pattern of change of the regular shape of land into other uses such as urban has prompted for adjustment in the structure of the environment, with high raised in temperature as compared to the rural areas around the environment. High

temperature is easily observed around the densely populated urban area and hence it prompted the formation of urban warmth island known as (UHI) (Ranagalage, M. and Weng, Q. 2004). The variation in temperature around the urban and rural areas is observed due to the loss of vegetation land, water land, and the transformation of land for farm into other uses which leads to the expansion in the land surface (Sharma, R. et al. 2015).

(Wang, R. and Ranagalage, M. 2018) suggested that the quick problem in LU/LC modelling has been created in the past and the information from those models enables us to investigate urban Geography, geomorphology, topography, and ecology through building up the possibility of urban variability and diversity of land use. The urban heat island phenomena and its impact on land use land cover is influenced by the urban pattern of city planning, the growth of the economy, developmental network of transportation and also enhance the environment. (Wang, R. 2018).

Geographic Information System and Remote Sensing have helped researchers around the world with latest techniques for managing the ecosystem. For the application of GIS/RS dataset has facilitated framework work/designing and variation at small medium and large scale for a long period of time. Those datasets have given significant association between local environmental studies, and management of local and international biodiversity (Wilkie and Finn, 1996).

Previously, dynamics relating to land use land cover have been modelled to for the acquisition of information for sustainable development (Ku, D. and Krajewski, P. et al. 2017).

Past research has shown that the interrelationship between the Land surface temperature (level of hotness the "surface" of Earth) and other indices such as normal difference vegetation index (NDVI) (Kumar, S. and Lee, L. et al. 2011), the land surface temperature (LST) and the normalized difference build-up index (NDBI) (Ranagalage, M. and Zhang, Y. 2018) was considered for the visualization of the true nature of the topography and landscape.

For the study of Mubi region, the spatiotemporal information from Landsat sources for four epochs of five years interval from (2004 to 2019) have been thoroughly studied and used to analyse the differences in LU/LC with respect to the UHI variation parameters over Mubi region, these were based on the summer season data (April–May) dataset.

This project area was chosen because Mubi is the second largest revenue generating local government area in the state and the rate of expansion, changes in the temperature level and increase in population has been observed over the year. As a result of variability in the dynamics of LU/LC parameters adjusted at the centre of the city and surroundings, its land resources are altered either directly or indirectly. The geospatial analysis must be applied to sustain the effects and protect future development of the Mubi region sustainable advancement.

This project design to investigate some of the interrelationship between LU/LC dynamics from 2004 to 2019 using Landsat Data to analyse the LST, NDVI, and NDBI at five years interval. Consequently, urban residential growth has an influence in the UHI as residents are considered elements of a specific geospatial multi-agent system. Mutual interactions of the Urban area, population growth and vegetation lost can help in determining the change in the LU/LC dynamics.

Regression analysis is one of the best tools to analyse the multiple datasets collected over a period of time. Studies have shown that Linear regression is a simple methodology for supervised learning. Linear regression has also been an important tool in evaluating a statistical data behaviour. It is an extremely clear methodology for forecasting a quantitative reaction of Y based on the X variable. The X and Y variables have a relationship that is linear. Using our Landsat dataset from the generated LST, NDVI and NDBI, we can come up with a linear relationship between those LU/LC dynamics.

It should be emphasized that for this project, the crucial assumption and the null hypothesis is that climate is changing and the global warming is impacting every part of the world, the temperature change in Mubi region was studied and investigated for 15 years dataset.

1.1 Problem Definition

The lack of maps and information depicting the geospatial distribution and the dynamics at the spatiotemporal level has prompted for this project the visualization of the relationship between the current UHI and how LU/LC is influenced by the NDVI, NDBI and LST spread around Mubi Region have been so difficult. This has necessitated the need to have a project that will graphically and statistically describe the LU/LC dynamics and pattern over the Mubi region. Also, advance analysis in statistics and Geospatial Science for depicting the spatiotemporal City model and building a regression model to find the correlation and the relationship between the LST, NDVI and NDBI has not been utilized in any previous research in my experience.

1.2 Research Questions

i. what is the mean temperature over the Mubi Region from 2004 to 2019 is it increasing or decreasing with the urban area increase or vegetation land increase?

ii. *How statistically significant is the correlation between the LST Vs NDVI and LST Vs NDBI and does this project help in accepting or rejecting the current null Hypothesis of UHI?*

II. Literature review

Spatiotemporal maps and statistical data are very crucial Information for land use/land cover study for spatial planning, management, and utilization of land for agriculture studies, and economic production (Abdulwahab A. et al, 2019).

Urban areas acquire various characteristics due to man-made activities on the surface of the earth, hence, it leads to a vast variety of topographic behaviour on the surface with respect to the radiation of longwave, the electromagnetic radiation absorbance evaporates and blocks the wind hence releasing heat to the urban area. (Bokaie, M. 2016).

Land surface temperature is not a universal indicator for soil moisture, scientist has shown that the level of hotness the earth "surface" in a specific location is experienced when touched is referred to as Land surface temperature. When the satellite sensor views the ground through the atmosphere, the most dominant information that is visualize is the surface. Some of this information could be ice, grass, snow, forest top, building top and another geomorphology. In this manner, the land surface temperature isn't equivalent to the air temperature that is incorporated into the everyday' weather forecasting

(https://earthobservatory.nasa.gov/globalmaps/MOD_LSTAD_M).

(Mirzaei, P, et al. 2015) suggest that the various materials for urban physical surface greatly vary, because they comprise asbestos, rock, stones, floor, ground surface, and solid materials, they minimize urban evapotranspiration and the rise the urban sensitivity. These are for the most part impacting the urban climatic condition. these lead to the urban areas getting hotter as compared to the outside areas, this is referred to as called surface urban heat island. According to (Babazadeh, M. and Joshi, R. et al 2015), the major elements that influence the atmosphere, human and animals drastically are the SUHI. It has been taking urban area at a significant level of temperature when compared with the temperature of the rural spaces due to growing in buildings developments on the landscape. (Avdan, U. and Rosa, A. 2017). The surface urban heat island has called on much professional attention in the consideration of surveyors, investors, planners, engineers and most community of researchers because of its advance consequences for the health of human just as on atmospheric properties such as quality of air, the balance of energy, urban temperature and the stored carbon. (Li, X. and Zhang, X 2017).

Previous research shows that land use land cover has been generated for acquisition of data relating to LC for urban sustainable development (Saarloos, D. and Wooldridge, M. 2011). Other research has shown that the relationship between the land surface temperature (LST) and normal difference vegetation index (NDVI) (Portugali, J. and Swan, M. et al. 2012) and LST/normalized difference buildup index (NDBI) can take into account the structure of the landscape for best visualization (Nowak, A. and Holyst, J. 2000).

There are many universal indicators of soil moisture apart from Land surface temperature. (Kamlesh K. & Kuldeep T,2011) suggested that LU/LC are significant parts of understanding the connectivity of humans and the landscape and in this manner, it is important to have the option of analysing change impacts. LU/LC has been accepted as a focal part of the strategy in natural resources management and systems of monitoring natural variation on earth surface.

There has been an interdisciplinary study of spatiotemporal modelling undertaken by the researchers that involve referencing numerous concepts and methods derived from environmental planning, geospatial planning, economic, spatial science, and mathematics or computer science. The problem of modelling Cities LU/LC change is the no availability of spatial information (Manonmani R. et al 2010). although, there have been numerous attempts at developing appropriate tools using modern technologies such as geospatial multi-agent system design and integration, agent-based systems, machine learning, data mining, augmented reality, virtual reality, or 3D models, to ensure effective participation of citizens in urban and territorial development decision-making with a game theoretical treatment (Batty, S. and Tan, R. 2016).

(Jacobs, J. 2016) points the correlation that exist between cities performance and the cities formation, e.g., the quality of life, vibrancy, and safety. (Zhang, Y. 2019), takes it a step further and shows the correlation that exist between cities performance and multiple aspects the urban form. The defined indexes represent 17 aspects of urban performance of a city district, grouped into four high-level indexes: Density, diversity, proximity, and energy. This same approach can be applied to determine the intercorrelation between the LST, NDVI, and NDBI within the interval of this project time series dataset.

Cellular automata (CA) have been effectively used in simulating urban variations and LU change. Several authors performed simulations of urban development and land-use changes using GIS-based cellular automata (Couclelis, H. and Hosseinali, F. 2012). (Li et al.2010) the use of "parallel computation techniques" shows drastic improvement in performing large-scale city simulation.

2.1 Aim and Objectives

The aim of this project is to model the Mubi region based on Landsat Spatiotemporal Dataset of (4 Epoch) using Geospatial Science techniques. The aim can be achieved through the objectives below:

- (i) The investigation of multitemporal LU/LC dynamics and find the correlation between the dynamics of the dataset;
- (ii) The extraction of the mean Land Surface Temperature for individual LU/LC dynamics and their effects from 2004-2019;
- (iii) The determination of LU/LC dynamics, like NDVI and NDBI, for the visualization of vegetation and build-up and the relationship with the land surface temperature of Mubi region;

2.2 The Project Scope

In light of the spatial dimension, the project was done within the Mubi region and it concentrated on the investigation of spatiotemporal City Modelling with Geospatial and GIS Techniques in the project area. The extent of this study consists of eight (8)

Wards with three (3) from Mubi south and five (5) from Mubi North Local Government Headquarters, namely: Digil, Gude, Kolere, Lamurde, Lokuwa Nasarawo, Sabon layi, and Yelwa. For this project, Landsat dataset of four (4) epoch were collected between April 2004 and May 2019. The temperature data within the study period was also investigated to determine the variation and correlations that exist within this period using the R and geographic information system tools environment. The parameters utilized as a piece of input information were gathered from various sources, it was based on five years interval from 2004 to 2019.

III. Methodology

In this project, we try to apply geospatial Science to investigate the relationship between LST of Mubi region, the NDVI, NDBI and the spatial order of the pattern. It is necessary to show that the issue of information asymmetry is of great importance for modeling the relationships between LST, NDV, and NDBI.

A reconnaissance study to understand the project area was carried out, the suitable Satellite image, X, Y coordinate of locations, was selected for various LU Categories, GCP's, temperature and ground truthing from Landsat metadata and ground dataset for the study.

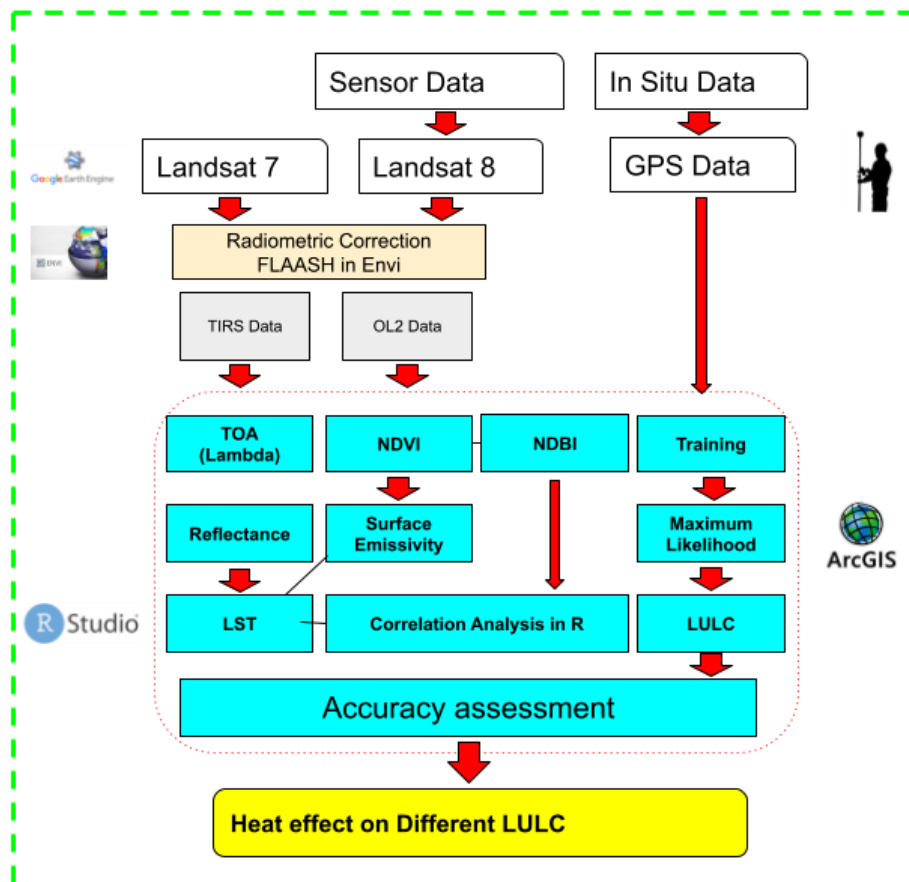


Figure 1a. Flowchart of the process

3.1 The Project Site

3.1.0 Site Description

“Mubi metropolis is a geopolitical area comprising of two local government areas; Mubi North and Mubi South. The metropolis is located between latitudes $10^{\circ} 05'$ and $10^{\circ} 30'N$ of the equator and between longitude $13^{\circ} 12'$ and $13^{\circ} 19'E$ of the Greenwich meridian. The two Local government areas occupy a land area of 192,307 Km² and support a total population of 260,009 people (National Population Census 2006). The area shares boundary with Maiha L.G.A in the South, Hong L.G.A in the West, Michika L.G.A and the Cameroon Republic in the East” (Adebayo 2004) as shown in (Figure 1b).

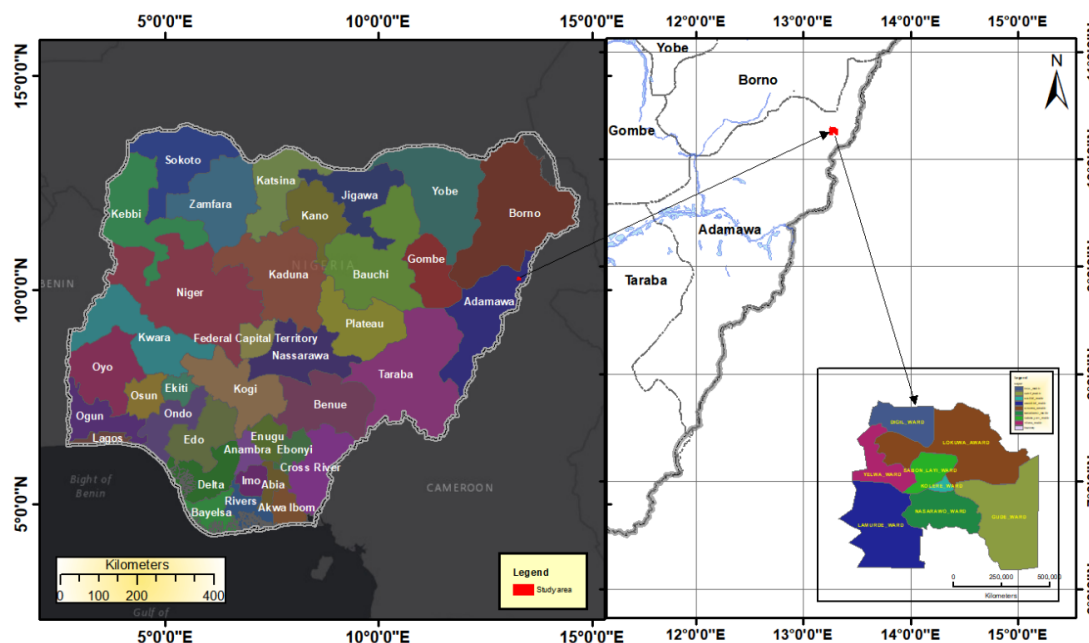


Figure 1b. Study area, a metropolitan Region, Mubi; (a) Mubi location in Adamawa State North-eastern Nigeria and (b) Map of Mubi with the regions surrounding the city Centre (Source: Surveying and Geoinformatics Federal Polytechnic Mubi).

3.2.0 Type and sources of data used

3.2.1 Landsat Dataset for this project work, an analysis was performed on images to evaluate the land use land cover dynamics over mubi region, the NDVI, LST and NDBI was analysed and the Landsat 7 images from 2004 to 2014 (ETM) was used while Landsat 8 image was used for 2019 image (OLI/ TRIS) data as shown in table (1). It was downloaded from (USGS) website (<https://earthexplorer.usgs.gov/> & <http://glovis.usgs.gov>). These were a pre-processed data from the source that has been corrected from atmospheric errors, geometric error, using the best algorithms, for image correction. In this project, 5 years interval dataset were analysed and detail visualization of the Urban Area (UL) with the large-scale expansion of urban development in Mubi Region; hence, 5-year intervals was the best approach in visualizing the variation in LU/LC change, in relation to the SUHI.

3.2.2 Landsat7/8 data

Landsat land use/landcover dataset was created through acquisition of Level 1 data of the Landsat 7 and 8 sensors datasets for the study of Mubi region. The pre-processing of the downloaded Landsat 7 and 8 data included five conceptual framework steps for the best presentation and the creation of accurate land-use land-cover maps. Step one was the geometric correction of the images based on the UTM/WGS 84 coordinate system, so as it will be in line with the dataset used for this project. The second step was that the digital numbers (pixel values) were converted to at-sensor radiance using information from the information in the metadata attached to the Landsat data.

After pre-processing, the Landsat 7 and 8 ETM images were ready to be used for the creation of the land-use land-cover maps (LU/LC). The basic criteria addressed for the final choice of the images intended to be used has been taken care of from cloud effects and other atmospheric factors before the download from the data source for all the four epochs of (2004,2009,2014 and2019). Due to the frequent cloud presence, spectral and textural features of the available Landsat 7 images were extracted, whenever these were available and cloud-free, and merged with the initial satellite images, resulting into various composite outputs.

In order to come up with the best classification accuracy for the project to be used producing the land use landcover map, a pixel-by-pixel sampling method was adopted for this project, resulting into the creation of random points around the vegetation class of the LU/LC being applied to the previously created composite images.

A sum of 32 points was selected for each of the periods of this project and the intermediate thematic maps were validated and statistical analysis was possible. Unsupervised classification from K-mean maximum likelihood iteration technique from ERDAS IMAGINE 2015 package was adopted to show six different classifications. These six classifications were categorized in to Fallow land cover (FL), Urban area (UL), vegetation cover, water (WB), Open space (OL) and Rock land (RL) to form a theme for the land-use land-cover maps of the project area (LU/LC). The type of datasets used in this project and sources can be found in table (1).

Table 1. Landsat data source for Mubi Region, a four epoch 5 years interval (2004–2019).

Sensors	ID of Scene	Date of Acquisition	period (GMT)	Thermal Band Infor	
				K1	K2
Landsat-7 ETM	LE07_L1TP_185053_20040427_20170121_01_T1	27 April 2004	09:14:12	666.09 (Band 6)	1282.71 (Band 6)
Landsat-7 ETM	LE07_L1TP_185053_20090527_20161221_01_T1	27 May 2009	09:15:30	666.09 (Band 6)	1282.71 (Band 6)
Landsat-7 ETM	LE07_L1TP_185053_20140525_20161115_01_T1	25 May 2014	09:22:25	666.09 (Band 6)	1282.71 (Band 6)
Landsat-8 OLI/TIRS	LC08_L1TP_185053_20190515_20190521_01_T1	15 May 2019	09:24:38	774.8853 (Band 10)	1321.0789 (Band 10)

Table 1b. Available field measurements per date and study area.

Study area	Date Measured	locations
Mubi region	27-Apr-04	32
Mubi region	27-May-09	32
Mubi region	25-May-14	32
Mubi region	15-May-19	32

Field data

For the spatiotemporal City modelling of Mubi Region, field measured data was acquired on the vegetations class for the project area epochs of 2004, 2009, 2014 and 2019 of landsat7 ETM and landsat8 TOI dataset downloaded. An overview of the dates of field measurements can be found in Table 4. In this project, these measurements were intended to be used for the validation of the accuracy assessment, correlation and regression model building to find the interrelationship between the LU/LC dynamics of LST, NDVI, and NDBI maps created at Landsat level (pixel resolution 30 m), since they are considered to be of very high accuracy.

For the sampling design, field surveys were performed in order to collect the information for training, validation and calibration of the products and models developed during the project. Therefore, Land Use Land Cover (LULC) data, as well as vegetation distribution within the Mubi region data was collected in representative locations of the project areas.

3.4 Information Extraction

For the extraction of LU/LC data, the Landsat images was employed representing the for four epochs, 2004 images, 2009 images, 2014 images, and 2019 images, on Mubi region Adamawa State. the LU/LC categories, Unsupervised classification using the K-mean maximum iteration technique on ERDAS IMAGINE 2015 package was adopted for showing the six (6) different categories. These six (6) categories were Urban area (UL), water (WB), Fallow cover (FL), vegetation cover (VL), Open Land (OL) and Rock land (RL).

“the analysis with Kappa is a discrete multivariate method use in precision investigation. The technique first introduced in 1981 for the remote sensing experts and it was initially published 1983 in the journal of remote

sensing journal. (Sexton, J. and Sultana, S.) says the Kappa coefficient can be used to calculate and indicate the level of classification accuracy. For this project, the kappa was utilized to discover the degree of matching between predefine value and the user define value” (Ishtiaque, A. 2017).

The classification accuracy check, known as, user accuracy, Kappa coefficient, overall accuracy, and producer accuracy, was executed using Eq1 to 4 respectively (Bokaie, M. and Pal, S. 2017):

$$Overall\ Accuracy = \left\{ \frac{\sum CCP(Diagonal)}{\sum CRP} * 100 \right\}, \quad (1)$$

C C P = Corrected Classified Pixels (diagonal);
C R P = Corrected Reference Pixels

$$User\ Accuracy = \left\{ \frac{\sum CCP(Category)}{\sum CPC(Row)} * 100 \right\}, \quad (2)$$

C C P (Category) = Corrected Classified Pixels (category)
C P C (Row) = Classified Pixels in a Category (the row total);

$$Producer\ Accuracy = \left\{ \frac{\sum CCP(Category)}{\sum CPC(Column)} * 100 \right\}, \quad (3)$$

C C P (Category) = Corrected Classified Pixels (diagonals)
C P C (Column) = Classified Pixels in that Category (Column Total);

$$Kappa\ Coefficients = \frac{N \sum_{i=1}^r X_{ii} \sum_{i=1}^r (X_{i+} * X_{+i})}{N^2 - \sum_{i=1}^r (X_{i+} * X_{+i})}, \quad (4)$$

where N = total samples r = number of rows in error matrix

X_{ii} = Total corrected samples in ith row and column

N² = Square of total samples

X_{i+} = column total X_{+i} = total row.

3.4.1 Land Surface Temperature (LST) Analysis and Extraction

Research has shown that the LST is the brightness temperature of the land surface, however, it does not represent the real temperature on the surface but it has a strong relationship with air temperature. Thus, LST could be an indicator for Urban Heat Island (UHI).

The Urban heat island (UHI) is a specific area of the build-up, generally in urban regions and it shows the locations where the environment is much hotter than the nearby unurbanized areas due to human activities.

When calculating the LST, we need the thermal bands (6) in ETM, and (10) in Landsat-8 dataset, it was then converted into radiance in Eq (5):

$$L_{\phi} = M_L * Q_{Cal} + A_L, \quad (5)$$

L_φ = Top of atmosphere (TOA) spectral radiance in (watts/(m² *sr*μm))

M_L = Multiplicative factor from metadata

Cal = Quantized and calibrated pixel values (DN) A_L = additive factor based from metadata.

The brightness temperature was calculated from Eq (6):

$$\tau = \left[\frac{K_2}{\ln\left(\frac{K_1}{L_{\phi}} + 1\right)} \right], \quad (6)$$

t = brightness temperature at the sensor,

L_φ = Top of atmosphere (TOA) spectral radiance in (watts/(m² *sr*μm)) K₁ and K₂ = Thermal constants from metadata (6 and 10) (Table 1). emissivity correction can be extracted from Eq (7)

LST (in Kelvin (K)) can be calculated from brightness temperature

$$\omega = \left[\frac{\tau}{1 + w\left(\frac{\tau}{p}\right) \ln(e)} \right], \quad (7)$$

“w = emitted radiance wavelength (11.5/10.8 μm for band 6/10) p = h × c/s 1.438 × 10⁻² mK) h is a Plank’s constant (6.626×10⁻³⁴ Js), s is the Boltzmann Constant (1.38×10⁻²³ J/K), and c is the velocity of light (2.988 × 10⁸ m/s). Equation (8) was employed for the extraction of land surface emissivity (e)

$$e = n P_v + m, \tag{8}$$

e = land surface emissivity, n = 0.004 and m = 0.986 and P_v is the proportion of vegetation (Ranagalage, M. 2017). Equation (9) was then incorporated for the extraction of the proportion of vegetation (P_v)”:

$$P_v = \left[\frac{NDVI - NDVI_{minimum}}{NDVI_{maximum} - NDVI_{minimum}} \right]^2, \tag{9}$$

P_v = proportion of vegetations.

For computation of NDVI, the reflectance data was extracted from R band and NIR band from Eq (10):

$$\rho^{\phi} = M_{\rho} Q_{Cal} + A_{Q}, \tag{10}$$

□ ϕ = TOA reflectance

ML = Multiplicative factor from metadata

Cal = Quantized and calibrated pixel values (DN) AL = additive factor based from metadata.

After the computation, the LST value was computed using Eq (11) (Avdan, U. and Sultana, S. 2018):

$$LST = LST(K) - 273.15. \tag{11}$$

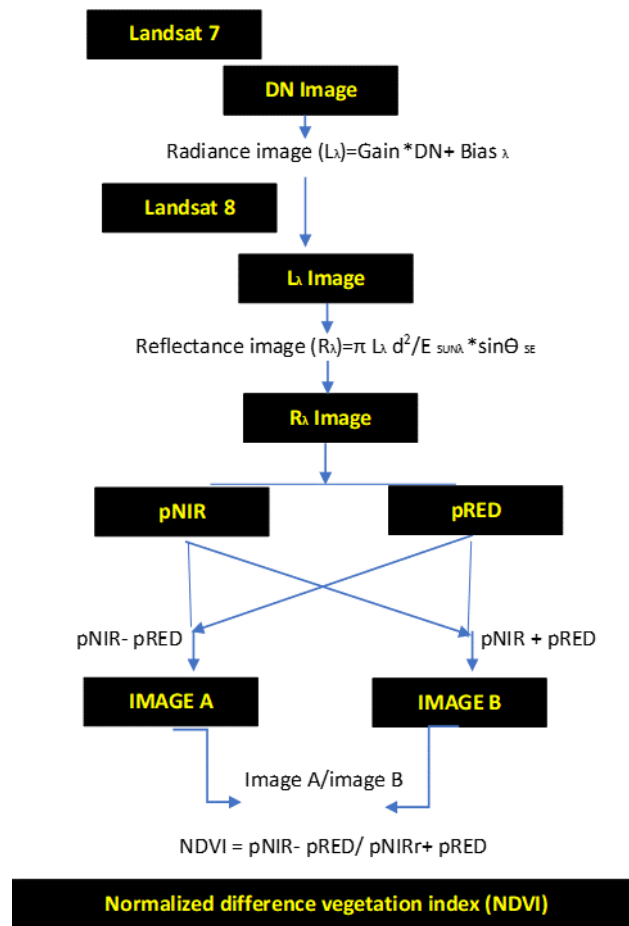


Fig. 3 Flowchart view of the NDVI Process.

NDVI Analysis and Extraction

The NDVI is a significant vegetation cover in light of the fact that the Seasonal and between yearly changes in vegetation development can be observed and monitored many types of multiplicative errors are present in different bands from various image dates (Jensen, J. 2009). Other studies indicate that “NDVI is one of the major indicators to understand the urban climate (Ranagalage, M. 2017). It ranges between -1 and +1,

where large positive values denote vegetation, small positive values denote built-up or bare soils, and negative to adjacent to negative values denote water bodies (Ranagalage, M. 2018). It provides information about vegetation abundance, phenology, and health (Pal, S. and Ziaul, S. 2017). NDVI was retrieved using Equation (12) through the red band and near-infrared (NIR) band” (Avdan, U. and Li, X. 2017):

$$NDVI = \left[\frac{NIR_{Band} - Red_{Band}}{NIR_{Band} + Red_{Band}} \right], \quad (12)$$

NDVI = Normalized Difference Vegetation Index (NDVI)

NIR band = Band 4 L7 (0.772–0.898 μm)

Band 5 OLI (0.85–0.88 μm)

RED band = Band 3 L7 (0.631–0.692) Band 4 OLI (0.636–0.673 μm).

3.4.3 NDBI Analysis and Extraction

“Many professionals working on urban/suburban problems are interested in monitoring the spatial distribution and growth of urban built-up areas. These data can be used for watershed runoff prediction and other planning applications. (Zha et al. 2003) calculated a Normalized Difference Built-up Index (NDBI):”

$$NDBI = Bu - NDVI \quad (13)$$

Where

$$Bu = (NIR_{TM4} - MidIR_{TM5}) / (NIR_{TM4} + MidIR_{TM5}) \quad (14)$$

“This resulted in an output image that contained only built-up and barren pixels having positive values while all other land cover had a value of 0 or ±254. The technique was reported to be 92% accurate”.

Research has also shown that the “NDBI is one of the major indicators to understand the urban climate (Ranagalage, M. 2017). It ranges from -1 to +1, where a large positive value denotes the built-up area, a small positive value denotes bare soils, and a negative value denotes water bodies and vegetation (Ranagalage, M. 2018). It provides information about the presence and extent of imperviousness (Pal, S. and Ziaul, S. 2017). NDBI was retrieved using Equation (15) through NIR band and mid-infrared (MIR) (Avdan, U. and Li, X. 2017). Before the calculation of NDBI, reflectance values of the NIR band and MIR band were extracted using Eq (10)”.

$$NDBI = \left[\frac{MIR_{Band} - NIR_{Band}}{MIR_{Band} + NIR_{Band}} \right], \quad (15)$$

MIR = band 5 (1.55–1.75 μm)

Band 6 OLI (1.57–1.65 μm)

NIR = Band 4 (0.76–0.90 μm) Band 5 OLI (0.85–0.88 μm).

3.5.0 Gradient Analysis of Urban-Rural

Studies have shown that the gradient technique can be applied for the assessment of the variation in temporal and spatial change in environment with respect to distance (Gunaalan, K. and Ranagalage, M. 2018). According to (Estoque, R. 2018), the gradient analysis can provide all the datasets relating to the spatial distribution of average land surface temperature, NDBI and NDVI and based on the gradient of cities and rural surrounding. It can also give some idea relating to the distribution of NDBI, NDVI and LST at city centre to the surrounding part of the urban landscape.

3.5.1 Introduction to Analysis In R

An analysis in R was performed to find the linear regression in the urban dynamics, the scattered plot and correlation between the variables of the four epochs, i.e., 2004, 2004, 2009, and 2019 between the land surface temperature and NDVI and land surface temperature and NDBI. In this analysis, the values of the pixels of LST, NDBI and NDVI was converted to get the data of the points (Ranagalage, M. 2017). The analysis was executed based on 128 points NDBI, LST and NDVI for the four years (2004, 2009, 2014, & 2019).

IV. Results and Discussion

The accuracy assessment of LU/LC category for Mubi Region was made in six different categories, viz Urban area (UL), Vegetation (VL), Water (WB), Fallow (FL), Rock (RL), and Open land Table (2). from this work, four epochs were analysed (2004, 2009, 2014, & 2019) based on unsupervised classification (K-mean) to show spatial distribution of the LU/LC variables, the LU/LC accuracy assessment for this project gives more than 92.00%.

Table 2. thematic classification of Mubi Region LU/LC.

No.	Category of LU/LC	Description LU/LC Class
1	UL	Urban Area (Impervious Land)
2	VL	Vegetation cover (Forested area)
3	WB	Water cover (open water, ponds, Lakes, reservoirs)
4	FL	Fallow Land (farm land and crops)
5	OL	Open space (barren land, abandoned land, bare land)
6	RL	Rock Land (Mountains, Stones)

Most of computerized image change investigations has been founded on processing date by date arrangement (n + 1) arrangement maps pixel by pixel. This, for the most, referred to as per-pixel change detection. On the other hand, object-based change detection (OBCD) includes the examination of at least two scenes comprising of numerous homogenous picture objects (known as patches) that were differentiated using object-based image Analysis (OBIA) method (Gartner et al., 2014).

(Jensen, J. 2009) suggested that the “change detection studies are overly ambitious in their attempt to monitor changes in the landscape. Sometimes the time period selected over which change is to be monitored is too short or too long to capture the information of interest”. hence, care must be taken when identifying change dynamics on various images over a period of time.

Given careful planning and sufficient resources “to obtain sufficient ground reference points at two dates in time, it is possible to populate the change detection error matrix with measurements. The major diagonal of the change matrix represented when the Date 1 classification of a pixel or polygon agrees with the Date 2 classification of the same pixel or polygon” (Jensen et al., 2012).

4.1 Spatiotemporal Modelling of Mubi Region LU/LC Dynamics (2004-2019)

Figure 3 shows the four epoch Landsat secondary datasets, the spatiotemporal LU/LC maps of Mubi Region were produced as depicted in Figure 4. The urban area (UL) class has been found to be expanding rapidly from all the other classes, as it was 888.527 Ha in 2004, then it increased by 1334.491 Ha in 2009; this class further increase to 1661.759 Ha in 2014, and at the end of the epoch analysis, the urban land class increases to 2325.782 Ha in 2019 as shown in (Table 3 and Figure 4) below.

Table 3. statistical summary of Mubi Region LU/LC from 2004- 2019 at 5 year interval.

Lu/Lc	Classes	2004	2009	2014	2019
S/n					
%					
		Ha	%	Ha	%
1	Urban area	888.527	16.88	1334.491	25.37
2	Vegetation	997.646	18.95	835.176	15.88
3	Water Body	216.448	4.11	87.635	1.67
4	Fallow Land	1140.154	1.66	1266.46	24.07
5	Open Land	1745.634	33.16	1632.129	31.03
6	Rock Land	276.423	5.25	104.643	1.99
	Total	5264.832	100	5260.534	100
		5260.535	100		

Hence the analysis shows that 1437.26 Ha i.e. 27.34% of the entire land and some LU/LC categories were changed into Urban Area class from 2004 - 2019 Table (4) & Figure (4). These analysis shows that water body WB category lost its area from 216.448 Ha 2004 to 74.208 Ha in 2019, this lost was 2.70% decrease within the period.

For the vegetation land, analysis shows that the Vegetation Land VL class lost its area from 997.646 Ha 2004 to 571.823 Ha in 2019, this lost was 8.08 % decrease within the period, most of this loss was due to gain in other dynamics of the LU/LC.

The fallow land class show lost in its area from 1140.154 Ha 2004 to 438.266 Ha in 2019, this lost was 13.32 % decrease within the period.

Open land class shows small lost in its area from 1745.634 Ha 2004 to 1742.143 Ha in 2019, this lost was 0.04 % decrease within the period which is almost a negligible loss in the open land.

Finally, the Rock land class show a loss in its area from 276.423 Ha 2004 to 108.313 Ha in 2019, this lost was 3.19 % decrease within the period of this study.

The LU/LC dynamics of this project has been analyzed for the four epochs of 2004, 2019, 2014 and 2019 as presented in (figure 4) below.

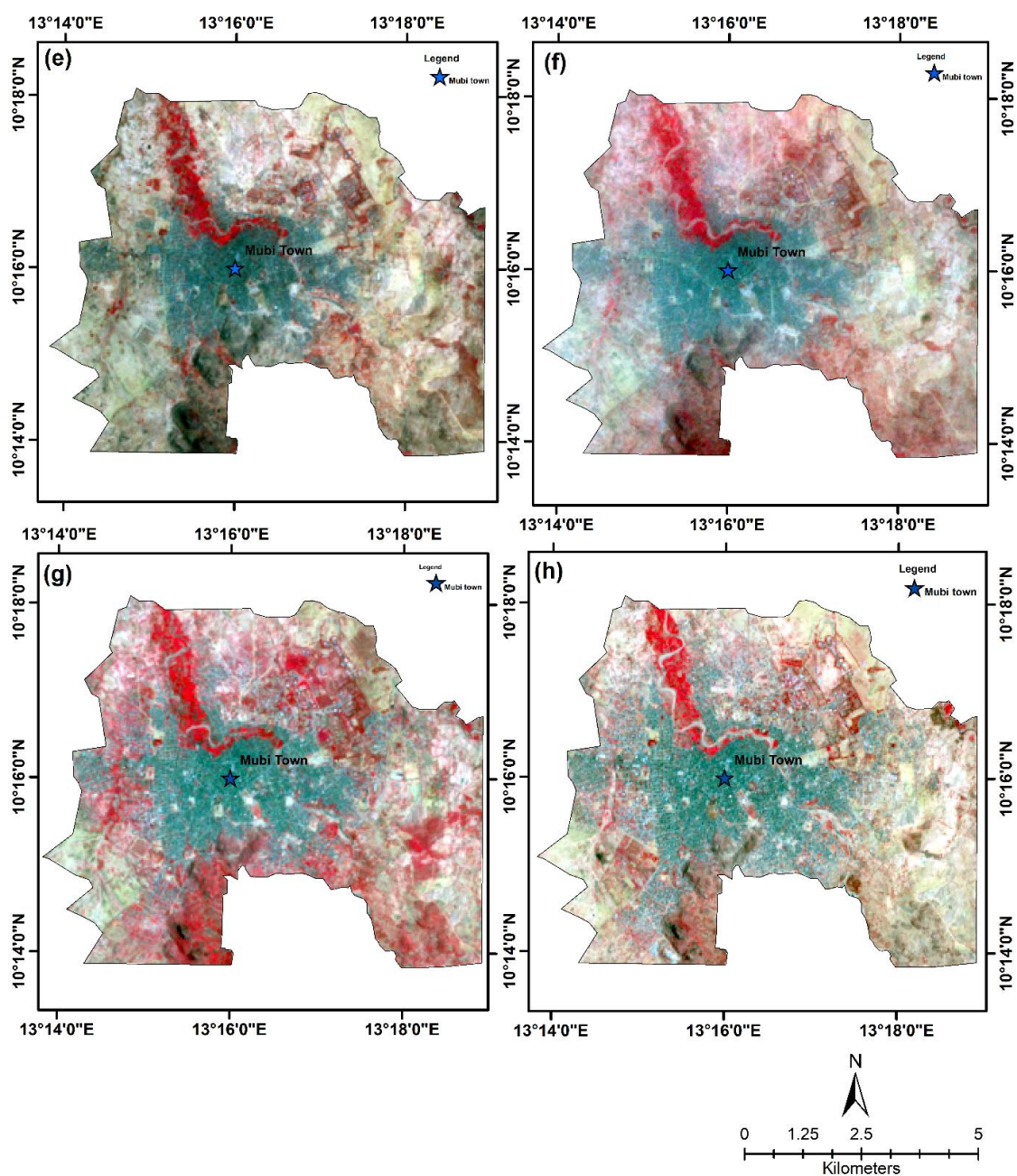


Figure 4. Four Epoch Landsat Image Over Mubi Region,
 (a) 27 April 2004, (b) 27 May 2009 of 1998, (c) 25 May 14 Over Mubi Region, (d) 15 May 19 Over Mubi Region.

The land use (LU) has tried to determine the major verity of activities being done within the Mubi region those activities have the potential to change from one class to another as those classes are dynamic. The land cover (LC) has tried to determine the how the landform is expanding and the extent of use of the land being done within the Mubi region those extents have the potential to change from one size to another as that cover is dynamic as presented in figure 5.

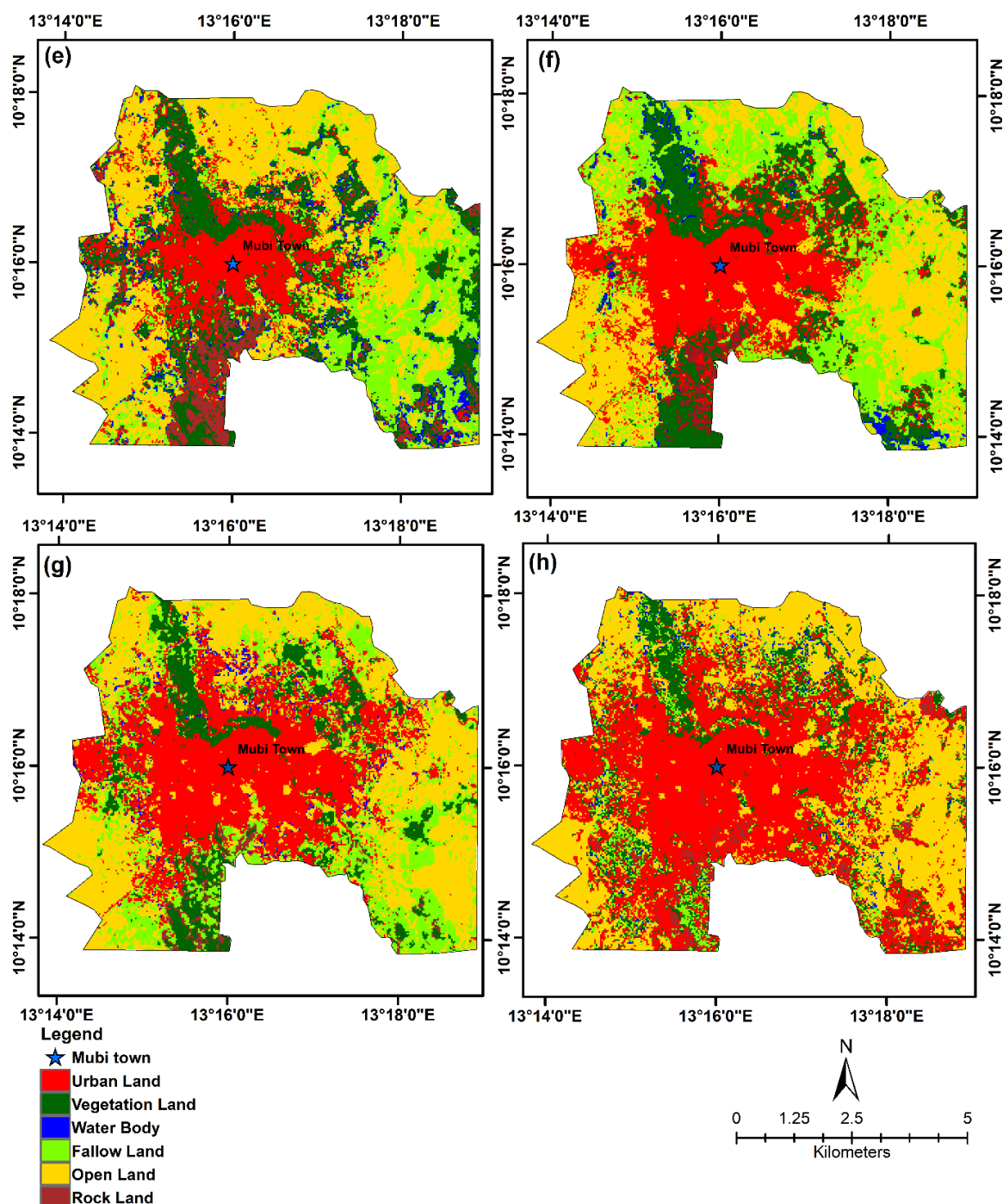


Figure 5. Spatiotemporal LU/LC dynamics model (a) 27 April 2004, (b) 27 May 2009 of 1998, (c) 25 May Over Mubi Region, a. LU/LC Maps of 2004 b. LU/LC 2014, and (d) 15 May 2019.

Table 4). Lu/Lc change statistical data of Mubi Region between 2004 - 2019 at 5-year intervals

S/n	LU/LC Classes	2004-2009		2009-2014		2014-2019		2004-2014		2004-2019		2009-2019	
		Ha	%	Ha	%	Ha	%	Ha	%	Ha	%	Ha	%
1	Urban	445.96	8.49	327.27	6.22	664.02	12.62	773.23	14.71	1437.26	27.34	991.29	18.84
2	Vegetation	162.47	3.07	-265.5	5.05	2.15	0.04	427.97	-8.12	-425.82	-8.08	263.35	-5.01
3	Water Body	128.81	2.45	-1.43	0.03	-12	-0.23	130.25	-2.47	-142.24	-2.7	-13.43	-0.26
4	Fallow Land	126.31	2.42	195.23	3.71	632.96	12.03	-68.93	-1.29	-701.89	13.32	828.19	15.74
5	Open Land	113.51	2.13	111.72	2.12	-1.7	-0.03	-1.79	-0.01	-3.49	-0.04	110.01	2.09
6	Rock Land	171.78	3.26	23.19	0.44	-19.52	-0.37	-148.6	-2.82	-168.11	-3.19	3.67	0.07

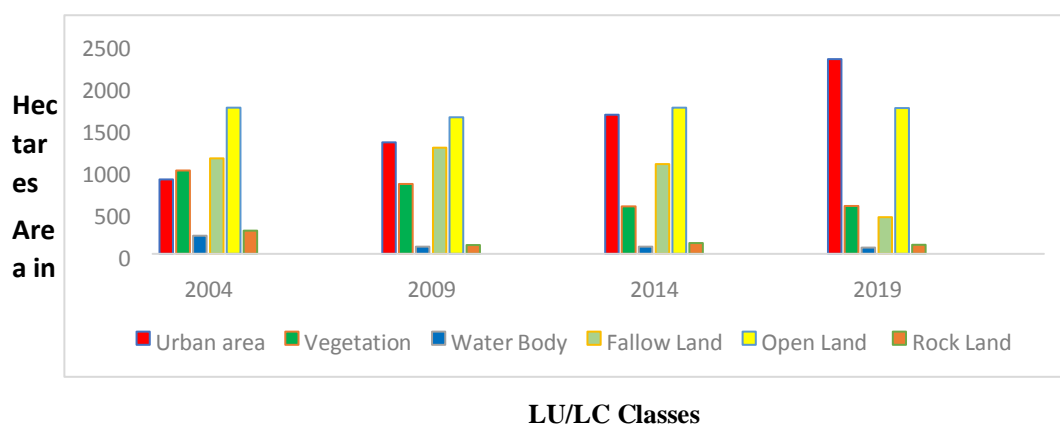


Figure 6. the LU/LC statistical graph of Mubi Region between 2004 - 2019 at 5-year intervals; area (in Ha).

4.2 Spatiotemporal Modelling of Mubi Region LST/SUHI Dynamics (2004-2019) Maps in figure 7 represent the SUHI maps of Mubi Region, this analysis was done for four epochs from Landsat datasets (2004, 2009, 2014, and 2019). the spatiotemporal model has taken into account the spatial pattern of the surface Urban heat island (SUHI). the statistical information relating to the model was shown in table 5. From this project, a maximum LST was observed on the western part of the region (Digil, Yelwa and Lamurde ward), the minimum was observed around the eastern part of the region (part of Lokuwa and Gude ward) for the 2004 dataset.

Table 5. Extracted statistical LST (°C) values Of Mubi Region for Four Epoch at 5-year intervals (2004–2019)

City	Date	Minimum	Maximum	Mean	Standard Deviation
		(°C)	(°C)	(°C)	
Mubi City	27-Apr-04	9.14	21.34	15.59	2.08
	27-May-09	15.56	23.63	20.16	0.89
	25-May-14	18.05	24.54	20.74	0.94
	15-May-19	20.41	27.8	24.88	0.96

For the 2009 dataset, maximum LST was observed on the western part of the region (part of Lokuwa and Gude ward), the minimum was observed around the northern and southern part of the region (part of Digil and Lamurde ward).

For the 2014 dataset, maximum LST was observed to be concentrated around the City centre, and all the surrounding region experience a lower temperature for Mubi region.

Finally, the 2019 dataset analysis shows a maximum LST on the eastern part of Mubi region and the city centre (Gude ward and Main City centre), the minimum was observed around the northern and southern part of the region (part of Digil and Lamurde ward and some part of Lokuwa ward).

The LST rise was as a result of Open Land (sandy type), and Urban Land (UL), respectively, while the major decline in LST was observed as a result of major vegetation land VL cover within of Mubi region as shown in (Figure 7 and 8) below.

The land surface temperature LST for the four epochs at the 5-year interval and it helps to visualize the variations in those periods. For the 2004 analysis in (Figure 7 and 9 (a)) it shows the value of the temperature ranges from 9.14–21.34 °C, it has a mean temperature of 15.59 °C at a standard deviation of 2.08 for that year.

The 2009 analysis shows that the value of the temperature ranges from 15.56–23.63 °C, it has a mean temperature of 20.16 °C at a standard deviation of 0.89 for 2009 in (Figure 7 and 9 (b)). From the 2014 analysis, we observed that the value of the temperature ranges from 18.05–

24.54 °C, it has a mean temperature of 20.74 °C at a standard deviation of 0.94 for 2014 in (Figure 7 and 9 (c)).

Finally, from the 2019 analysis, we observed that the value of the temperature ranges from 20.41–27.8 °C, it has a mean temperature of 24.88 °C at a standard deviation of 0.96 for 2019.

The maximum mean temperature variation between 2004 and 2019 was found to be 9.29 °C for 2019 as shown (Figure 7 and 9 (d))

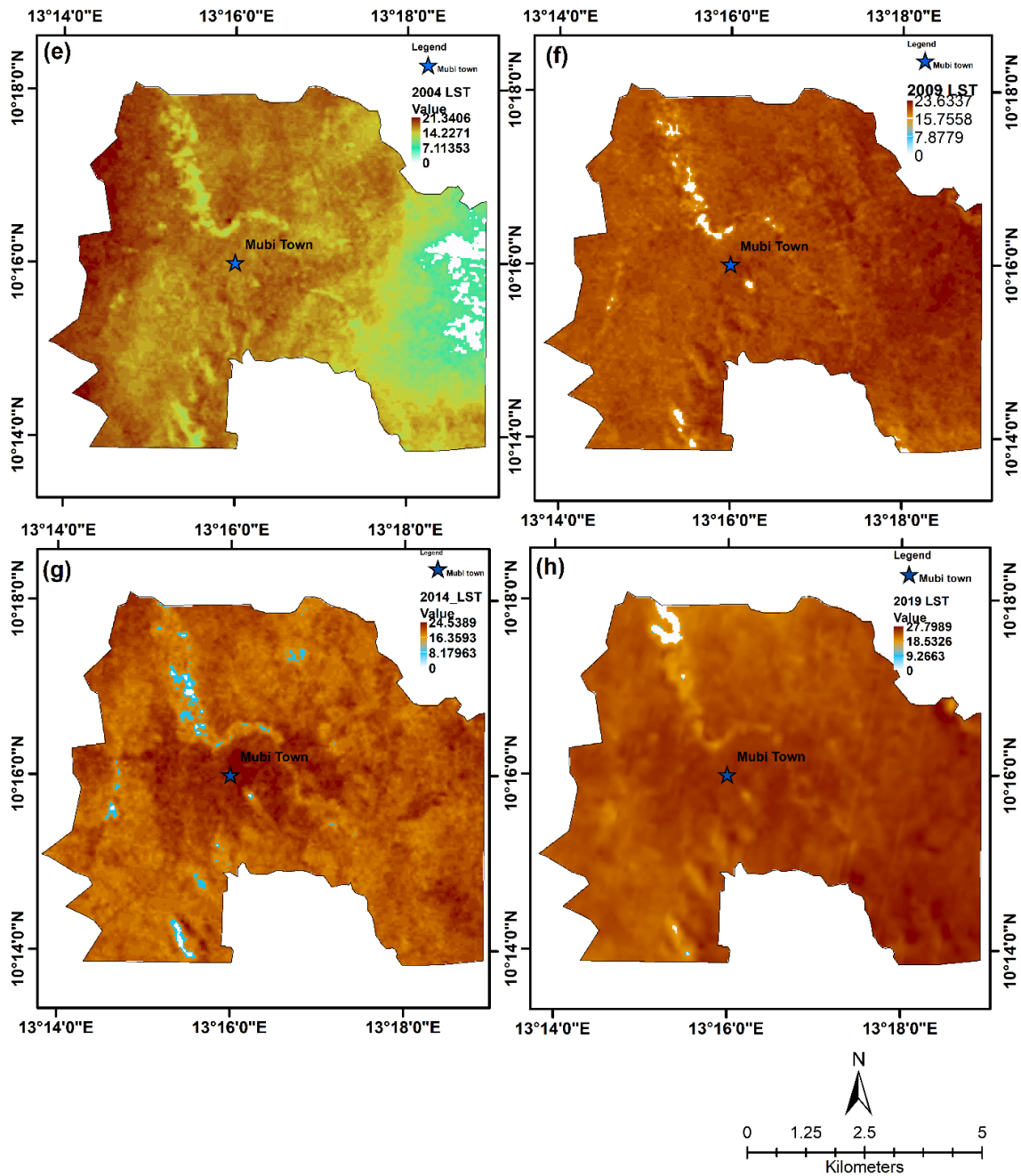


Figure 9. 20 years LST Variation Over Mubi Region, (a) 27 April 2004, (b) 27 May 2009 of 1998, (c) 25 May 2014, and (d) 15 May 2019.

Spatiotemporal Modelling of Mubi Region NDVI Dynamics from (2004-2019)

In this project, the NDVI maps of Mubi region was created as depicted in Figure 9, the four epochs Landsat image dataset (2004, 2009, 2014, and 2019) were analyzed and take into consideration the spatial pattern to model the NDVI distribution; table 7 shows the univariate statistical information for the period of the project. From the analysis, figure 10c 2014 experience the highest NDVI mean value of 0.25, then it decreased to 0.23 in 2019 figure 10d the difference is 0.02 which is a very negligible difference.

Table 7. Retrieved statistics of NDVI values Of Mubi Region for the Four Epoch at 5-year intervals (2004–2019)

Date					
City		Minimum	Maximum)	Mean	Standard Deviation
Mubi City	27-Apr-04	-0.17	0.3	-0.06	0.04
	27-May-09	0.08	0.32	0.17	0.03
	25-May-14	0.01	0.64	0.25	0.09
	15-May-19	0.04	0.7	0.23	0.08

The beginning epoch shows a very low mean value of 0.06 NDVI for 2004 figure 10a, then the average NDVI increased up by 0.17 during 2009, and further rise by 0.25 which is the maximum NDVI year (2014) then finally decreases to 0.23 Value at the last epoch of the analysis 2019 (Table 8).

Table 8. Retrieved statistics of NDBI values Of Mubi Region for the Four Epoch at 5-year intervals (2004–2019)

City	Date	Minimum	Maximum)	Mean	Standard Deviation
Mubi City	27-Apr-04	0.97	0.99	0.98	0
	27-May-09	0.96	0.98	0.97	0
	25-May-14	0.93	0.98	0.97	0
	15-May-19	-0.4	0.35	0.07	0.06

Figure 9 shows the time series of the mean variation between the NDVI values from the Landsat image dataset analysis of Mubi region. As the NDVI Start from -1 to +1, the starting epoch 2004 starts with a negative mean value of -0.06, the minimum standard deviation was observed from the analysis of 2009 (0.03) dataset while the maximum standard deviation was observed in the result of the 2014 analysis.

The highest distribution of NDVI was observed at the north-western part of the project area and they are concentrated towards the streamline as it has a more conducive atmosphere for their growth in the region, however, the NDVI was lowest on the build-ups area which shows brighter parts of the region at all consecutive epochs (2004–2019).

Table 9. NDVI, NDBI and LST datasets from 2004 to 2019 of Mubi Region.

id	2004ndvi	2004lst	2004ndbi	2009ndvi	2009lst	2009ndbi	2014ndvi	2014lst	2014ndbi	2019ndvi	2019lst	2019ndbi	x	y
ID1	-0.064	13.686	0.986	0.208	18.054	0.974	0.367	19.943	0.97	0.226	24.869	0.115	313758.7	1131802
ID2	-0.05	18.529	0.985	0.154	19.474	0.975	0.26	21.341	0.974	0.232	24.901	0.064	307649.2	1135687
ID3	-0.016	15.648	0.984	0.167	19.474	0.973	0.28	20.877	0.97	0.248	24.629	0.049	309236.5	1134103
ID4	-0.099	17.098	0.985	0.131	20.411	0.973	0.115	22.263	0.976	0.174	25.512	0.057	312171.5	1135389
ID5	0.033	16.617	0.983	0.218	19.474	0.971	0.181	20.411	0.968	0.169	25.04	0.097	309685.7	1136554
ID6	-0.046	10.676	0.986	0.157	21.341	0.977	0.217	20.877	0.977	0.214	25.595	0.127	315136.4	1133685
ID7	0.121	15.648	0.981	0.223	19.943	0.973	0.336	19.474	0.975	0.318	24.052	0.036	308757.3	1137899
ID8	0.035	15.648	0.982	0.218	19.003	0.971	0.444	19.943	0.955	0.581	24.035	-0.249	310883.7	1136435
ID9	0.164	13.19	0.976	0.286	16.617	0.964	0.518	19.003	0.947	0.64	22.884	-0.338	309536	1136823
ID10	-0.067	18.054	0.984	0.146	19.003	0.973	0.184	20.877	0.974	0.164	24.82	0.074	307499.5	1135269
ID11	0.047	14.671	0.981	0.234	19.003	0.972	0.5	19.943	0.959	0.554	22.544	-0.279	309146.6	1137840
ID12	-0.085	17.577	0.985	0.147	19.943	0.973	0.17	21.803	0.974	0.149	25.329	0.013	310075	1136584
ID13	0.013	15.648	0.983	0.198	19.943	0.972	0.288	21.341	0.971	0.26	24.528	-0.053	312740.5	1137600
ID14	-0.038	16.617	0.983	0.179	20.411	0.974	0.246	19.943	0.973	0.24	24.444	0.093	310524.3	1136883
ID15	-0.05	10.166	0.984	0.16	22.263	0.974	0.223	20.877	0.977	0.213	25.793	0.099	314597.3	1135628
ID16	-0.073	17.098	0.984	0.182	19.474	0.972	0.214	20.877	0.972	0.247	24.85	0.035	309775.6	1136823
ID17	-0.013	15.161	0.984	0.973	19.474	0.973	0.463	19.474	0.963	0.451	23.886	-0.046	309416.2	1131862
ID18	-0.037	12.692	0.984	0.208	17.098	0.971	0.399	18.054	0.967	0.388	21.675	-0.023	309296.4	1131652
ID19	-0.054	14.18	0.985	0.203	19.943	0.975	0.366	20.411	0.972	0.225	25.903	0.14	314237.9	1132549
ID20	0.034	15.648	0.983	0.27	18.054	0.969	0.444	19.003	0.961	0.528	20.917	-0.137	309026.8	1138676
ID21	-0.087	15.648	0.984	0.141	19.943	0.975	0.113	22.263	0.978	0.149	25.674	0.059	311542.5	1134462
ID22	-0.068	14.671	0.986	0.187	19.943	0.975	0.39	19.943	0.97	0.222	25.914	0.131	314357.7	1132340
ID23	-0.071	16.133	0.985	0.16	19.003	0.974	0.3	21.341	0.968	0.188	24.58	0.069	309146.6	1132997
ID24	-0.042	13.686	0.985	0.202	18.054	0.973	0.335	19.474	0.974	0.293	22.853	0.07	309386.2	1131772
ID25	0.046	15.161	0.982	0.271	18.054	0.969	0.3	19.474	0.963	0.269	22.038	-0.064	308996.9	1138467
ID26	0.019	13.19	0.981	0.183	19.003	0.971	0.252	20.411	0.972	0.208	25.431	0.107	312740.5	1133535
ID27	-117	19.003	0.985	0.118	19.943	0.975	0.14	22.722	0.975	0.164	25.491	0.079	307050.2	1135628
ID28	-0.007	10.676	0.984	0.157	21.341	0.977	0.208	20.877	0.977	0.187	25.561	0.129	315076.5	1133715
ID29	0.038	16.133	0.983	0.227	19.003	0.972	0.292	19.003	0.969	0.191	24.007	0.013	308847.2	1137571
ID30	-0.117	16.133	0.985	0.114	19.943	0.974	0.127	21.341	0.973	0.12	25.115	0.069	308966.9	1133894
ID31	-0.07	12.191	0.984	0.158	21.341	0.975	0.231	21.341	0.972	0.186	25.616	0.09	314627.2	1135299
ID32	-0.068	16.133	0.985	0.171	19.943	0.974	0.202	20.877	0.974	0.159	24.801	0.07	309236.5	1133027

Spatiotemporal Modelling of Mubi Region NDBI Dynamics from (2004-2019)

The NDBI maps of Mubi region was created as depicted in Figure 12, the four epochs Landsat image dataset (2004, 2009, 2014, and 2019) were analysed and take into consideration the spatial pattern to model the NDVI distribution; table 8 shows the univariate statistical information for the period of the project. From the analysis, figure 12a 2004 shows that the NDBI ranges from 0.972 to 0.988 hence the increased difference in the Build-up is 0.0160 for

2004 at 1.9%, as a result, it amounts to the minimum increment of all the years. figure 12b 2009 shows that the NDBI ranges from 0.961 to 0.988 hence the increased difference in the Build-up is 0.0180 for 2009 at 2.2%. figure 12c 2014 shows that the NDBI ranges from 0.935 to 0.984 hence the increased difference in the Build-up is 0.049 for 2014 at 5.9%.

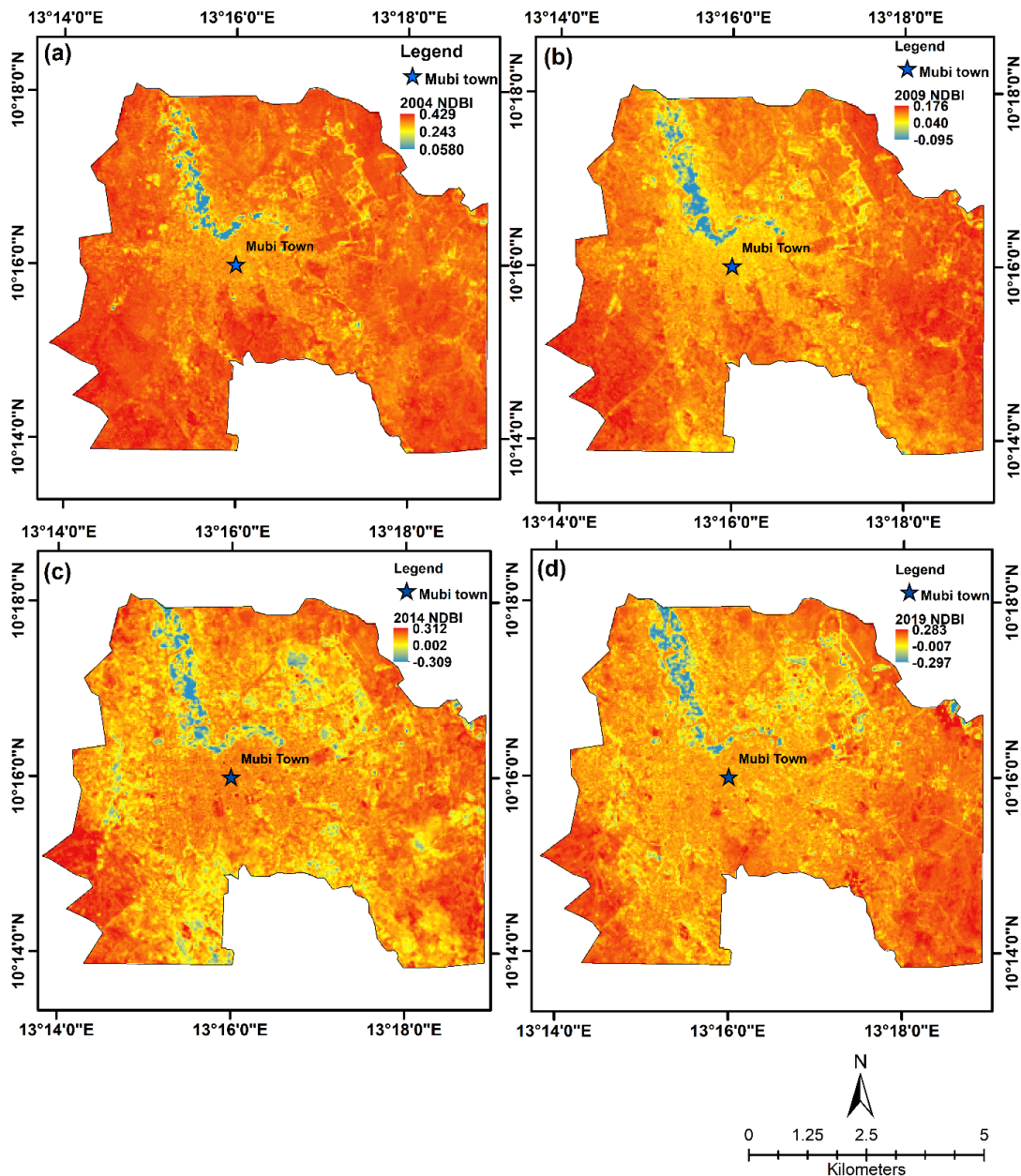


Figure 10. Spatiotemporal NDBI dynamics Model Over Mubi region, a) NDBI Maps of 2004 b) NDBI Map of 2009 c) NDBI Maps of 2014 & d) NDBI Maps of 2019.

figure 12d 2019 shows that the NDBI ranges from -0.401 to 0.348 hence the increased difference in the Build-up land is 0.749 which amount to 90% and the maximum increase of all the years. The reason for this increment between 2014 to 2019 was due to population growth as a result of insurgency attack at the end of 2014 in the neighboring local governments as a result of Boko Haram, and Mubi being the second largest local government in the state attracts a lot of commercial activities from Cameroon and Chad. Furthermore, the security level of Mubi is much more safe and secure as compare to the other local governments around the Mubi region of Adamawa state.

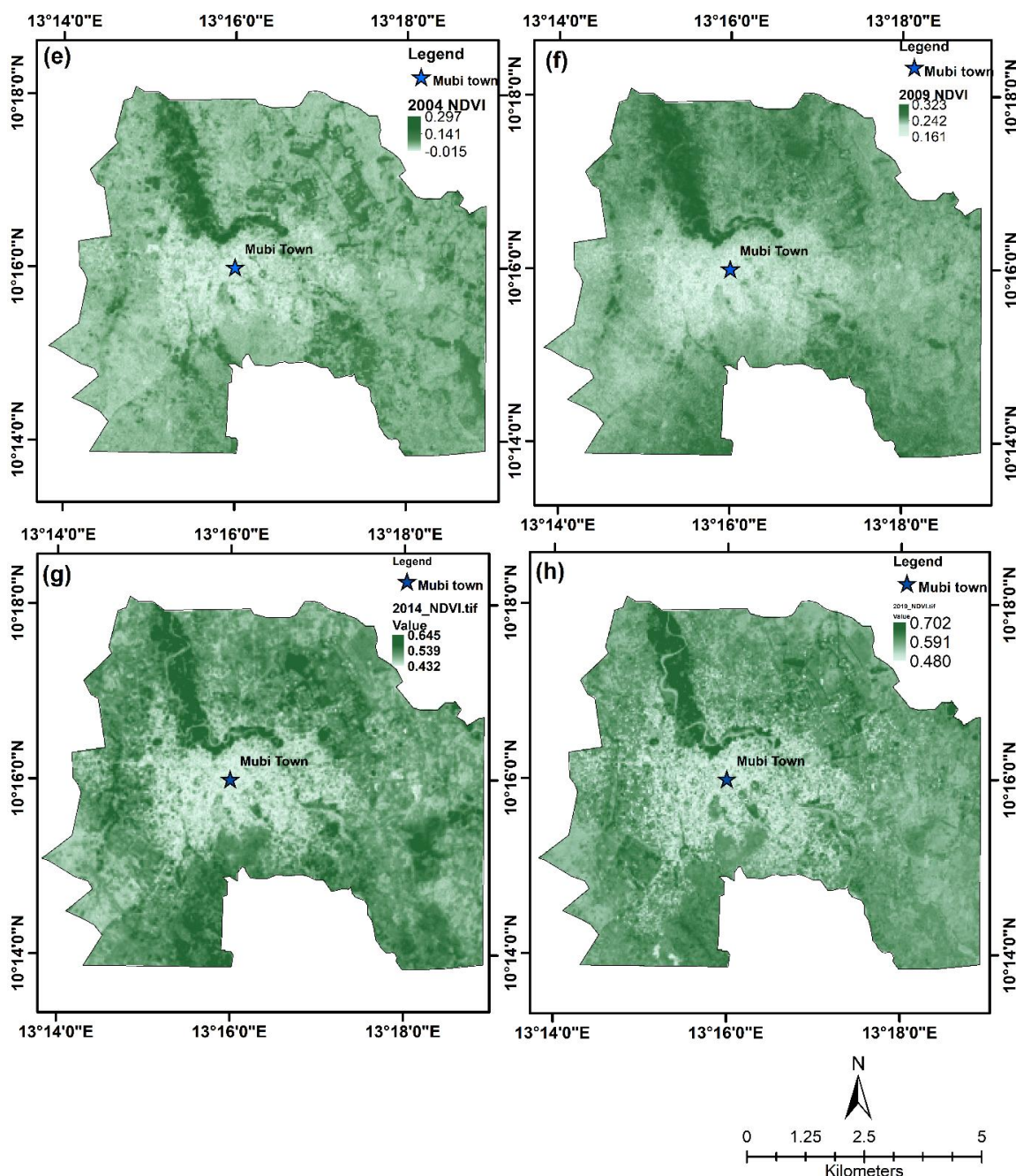
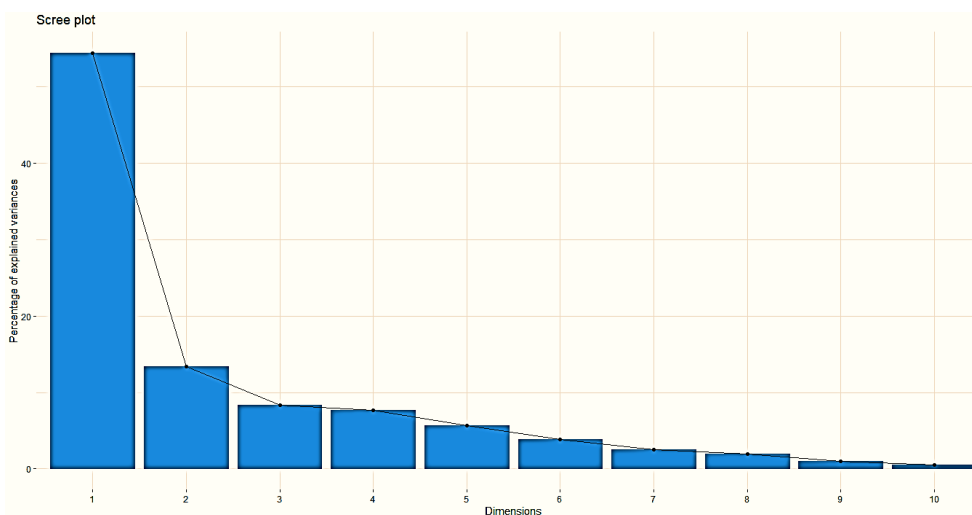
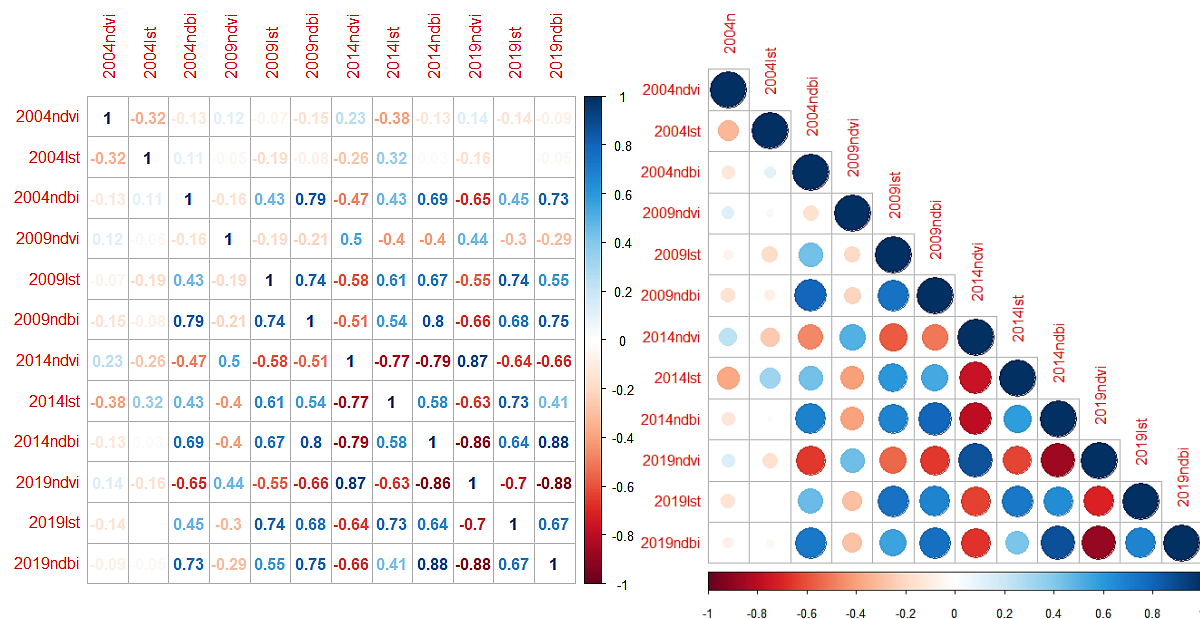


Figure 9. Spatiotemporal NDVI dynamics Model Over Mubi region, a) NDVI Maps of 2004 b) NDVI Map of 2009 c) NDVI Maps of 2014 & d) NDVI Maps of 2019.

Spatiotemporal Raster Modelling Analysis in R programming

R is an open source free statistical and programming software used for reading, visualizing, analyzing, modelling interpreting, manipulating and writing of spatial data that are gridded such as vector and raster dataset. R implements the basic of high-level language. It also Process and supports large files. For this project, we attempt to take advantage of the R package to analysis the raster images of the Mubi region for four epochs of 2004, 2009, 2014, and 2019 respectively. The R allows for visualizing the bands of each year at one go, selecting the suitable bands for modelling the normalized difference vegetation index (NDVI), the normalized build-up index (NDBI) and the land surface temperature (LST).

The R makes the statistical analysis on the dataset possible for this project. We run the Principal component analysis (PCA) to transforms a number of (possibly) correlated variables (Table 9) from (2004-2019) to a number of smaller uncorrelated PC's variables. We observed that the first PC takes 54.4% in the dataset, while the second principal components account for 13.4% as show figure 13.



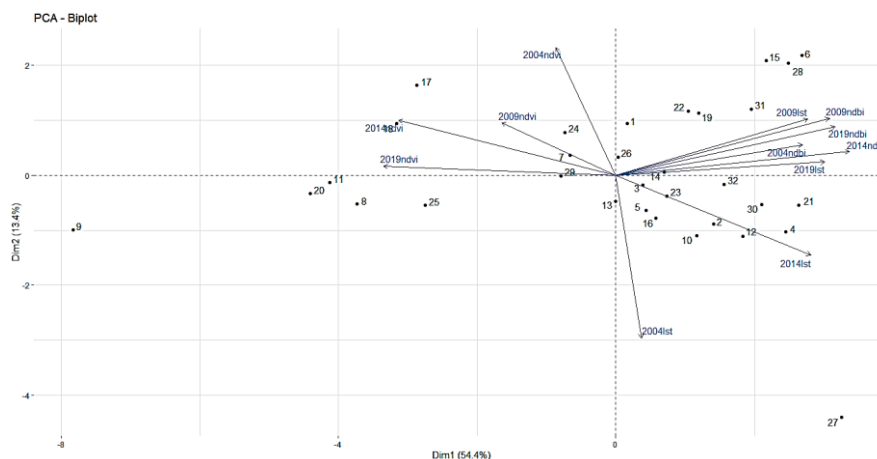


Figure 13. principal component analysis output and correlations between NDVI, NDBI and LST dataset from the project.

SPATIOTEMPORAL MODEL OF MUBI NDBI DYNAMICS WITH RESPECT TO LST FROM R

this analysis was done to investigate the interrelationship between the NDBI and the LST, it was observed that the correlation between NDBI and the LST was found to be positive throughout the four epoch, as shown in Figure 17, the R^2 value for 2004,2009,2014 and 2019 was found to be 0.01,0.55,0.34 and 0.45 and the P-value increases at each of the time-point period, as it was 0.57 in 2004, 1.25810^{-06} in 2009, 4.97×10^{-04} in 2014, and 2.397×10^{-05} in 2019 (Figure 18). We can deduct from this project that a positive correlation between LST and NDBI, shows that the LST increases as the NDBI increased in all the epoch, and this relationship showed that due to the rapid building development within the project area, the LST tend to increased (Table 9). Hence the surface Urban heat Island (SUHI) is highly influenced by the level of urbanization and population increase.

4.7 SPATIOTEMPORAL MODEL OF MUBI NDVI DYNAMICS WITH RESPECT TO LST FROM R

From this analysis, it was observed that the correlation of the NDVI with respect to the LST was negative throughout the four epoch, as shown in Figure 18, the R^2 value for 2004,2009,2014 and 2019 was found to be 0.10,0.04,0.59 and 0.50 and the P-value goes down on each of the epoch, it was found to be 0.07 (2004), 0.29 (2009), 2.84×10^{-07} (2014), and 6.748×10^{-06} in 2019 (Figure 18). We can deduct from this project that a negative correlation between LST and NDVI, shows that the NDVI is negative when the LST rises in all the epoch, the relationship was observed as the result of lower vegetation in the project, the LST rised

V. Conclusion

I will like to conclude that this project was executed through four (4) epoch of five years spatiotemporal analyses ranging from 2004 to 2019. The result of this project depicts that the urban area has expanded by 1437.26 Hectares (27.34%) and vegetated land was reduced by 425.82 Hectares (-8.08%), the water body reduced by 142.24 hectares (-2.70%), fallow land reduces by 701.888 hectares (-13.32%), open land reduced by 3.491 hectares (-0.04%) and the rock land was also reduced by 168.11 hectares (-3.19%) respectively. from the period of this project, we observe that all the land uses lost their sizes except the urban area which increases by a large percentage. The mean land surface temperature (LST) for 2004 was 15.59°C then it increases to 20.16°C in 2009. it further increases to 20.74°C and finally rises to 24.88°C . the mean increase for the four epochs was observed as a result of urban area growth as demonstrated from the R statistical analyses of this project.

The R has help in this analysis to investigate the relationship between the NDVI, NDBI, and LST from 2004-2019 as presented in the results (figure 13). We confirm from this project that positive correlation exists between LST & NDBI exist, and this shows that the LST increases as the NDBI increased in all the epoch from 2004-2019, and this relationship showed that due to the rapid building development within the project area, the LST tend to increased (Table 9). Hence the surface Urban heat Island (SUHI) is highly influenced by the level of urbanization and population increase. furthermore, a negative correlation between LST and NDVI, exist between the NDVI and LST hence NDVI falls as the LST rises in all the epoch of 2004-2019. The relationship was established because of the presences of less vegetation cover.

Hence lower vegetation higher LST and higher vegetation lower LST and vice versa. Finally, we can conclude that the main objectives of this project have been captured i.e. situation and geospatial dynamics in terms of LU/LC phenomena, the surface urban heat island SUHI, and also the correlations between the NDVI, NDBI with respect to the land surface temperature (LST) in Mubi region for four epochs from 2004-2019 at five years interval. This project has enhanced the information about the landform for a period of 15 years. Very

effective strategies, policies, and planning can be derived and developed based on this project to incorporate the rate of Mubi region growth based on urban land, the lost in of vegetation-land use, deplete in open land, lost in fallow land, and lost in the extent of the water bodies in the project area.

Acknowledgements

This research was funded by the **Tertiary Education Trust Fund (TETFUND)** under the institutional-based research Federal Polytechnic Mubi. We thank The U.S. Landsat project management, USGS Earth Resources Observation and Science (EROS) Center and CRAN for providing us with images and open-source programming software used in this study. The anonymous reviewers are thanked for their positive comments.

Reference

- [1]. Abdulwahab, A. Abdulganiyu, A. and Bello, A. (2019). Geospatial Modelling of Land Use/Land Cover Change Detection, Remote sensing and GIScience approach: Adamawa State University Mubi, Nigeria. *IOSR Journal of Environmental Science, Toxicology and Food Technology (IOSR-JESTFT) e-ISSN: 2319-2402,p- ISSN: 2319-2399. Volume 13, Issue 3 Ser. II (March. 2019), PP 21-29.* DOI: 10.9790/2402-1303022129
- [2]. Adebayo, A. A., and Musa, A. A (2004): Using the GIS to map areas suitable for upland rice production in Adamawa state: a paper presented at the School of Environmental Science, F.U.T. Yola. pp: 2-4
- [3]. Avdan, U.; Jovanovska, G. (2016). Algorithm for automated mapping of the land surface temperature using Landsat 8 satellite data. *J. Sens.* 1–8. [CrossRef]
- [4]. Babazadeh, M.; Kumar, P. (2015). Estimation of the urban heat island in local climate change and vulnerability assessment for air quality in Delhi. *Eur. Sci. J.* 19, 55–65.
- [5]. Batty, S.E. (1977). Game-Theoretic Approaches to Urban Planning and Design. *Environ. Plan. B Urban Anal. City* 4, 211–239. [CrossRef]
- [6]. Bokaie, M.; Zarkesh, M.K.; Arasteh, P.D.; Hosseini, A. (2016). Assessment of urban heat island based on the relationship between land surface temperature and land use/land cover in Tehran. *Sustain. Cities Soc.* 23, 94–104. [CrossRef]
- [7]. Couclelis, H. (1997). From cellular automata models to urban models: New principles for model development and implementation. *Environ. Plan. B* 24, 165–174. [CrossRef]
- [8]. Estoque, R.C.; Pontius, R.G.; Murayama, Y.; Hou, H.; Thapa, R.B.; Lasco, R.D.; Villar, M.A. (2018). Simultaneous comparison and assessment of eight remotely sensed maps of Philippine forests. *Int. J. Appl. Earth Obs. Geoinf.* 67, 123–134. [CrossRef]
- [9]. Estoque, R.C. Murayama, Y. Myint, S.W. (2017). Effects of landscape composition and pattern on land surface temperature: An urban heat island study in the megacities of Southeast Asia. *Sci. Total Environ.*, 577, 349–359. [CrossRef]
- [10]. Gartner, P., Forster, M., Kurban, A., and B. Kleinschmit, 2014, "Object Based Change Detection of Central Asian Tugai Vegetation with Very High Spatial Resolution Satellite Imagery," *International Journal of Applied Earth Observation and Geoinformation*, 31:110±121.
- [12]. Gunaalan, K.; Ranagalage, M.; Gunarathna, M.H.J.P.; Kumari, M.K.N.; Vithanage, M.;
- [13]. Srivaratharasan, T.; Saravanan, S.; Warnasuriya, T.W.S. (2018). Application of geospatial techniques for groundwater quality and availability assessment: A case study in Jaffna Peninsula, Sri Lanka. *ISPRS Int. J. Geo-Inf.* 7, 20. [CrossRef]
- [14]. Hosseinali, F.; Alesheikh, A.A.; Nourian, F. (2012). Simulation of Land-Use Development, Using a Risk-Regarding Agent-Based Model. *Adv. Artif. Intell.* 2012. [CrossRef]
- [15]. Holyst, J.A.; Kacperski, K.; Schweitzer, F. (2000). Phase transitions in social impact models of opinion formation. *Phys. A Stat. Mech. Appl.* 285, 199–210. [CrossRef]
- [16]. Iman, R. Omar S. Rajan D. Haraldur O. Manjula R. (2018). Spatiotemporal Analysis of Land Use/Land Cover and Its Effects on Surface Urban Heat Island Using Landsat Data: A Case Study of Metropolitan City Tehran (1988–2018)
- [17]. Ishtiaque, A.; Shrestha, M.; Chhetri, N. (2017). Rapid urban growth in the Kathmandu valley,
- [18]. Nepal: Monitoring land use land cover dynamics of a Himalayan city with Landsat imageries. *Environments* 4, 72. [CrossRef]
- [19]. Jacobs, J. *The Death and Life of Great American Cities*; Vintage: New York, NY, USA, 2016.
- [20]. Jensen, J. R., Im, J., Hardin, P., and R. R. Jensen, 2009, "Chapter 19: Image Classification," in *The Sage Handbook of Remote Sensing*, Warner, T. A., Nellis, M. D. and G. M. Foody, (Eds.), 269–296.
- [22]. Jensen, R. R. and J. M. Shumway, (2010). "Sampling Our World," in G Gomez, B., and J. P.
- [23]. Jones III (Eds.), *Research Methods in Geography*, NY: Wiley Blackwell, 77± 90.
- [24]. Joshi, R.; Raval, H.; Pathak, M.; Prajapati, S.; Patel, A.; Singh, V.; Kalubarme, M.H. (2015). Urban heat island characterization and isotherm mapping using geo-informatics technology in Ahmedabad city, Gujarat state, India. *Int. J. Geosci.* 6, 274–285. [CrossRef]
- [26]. Krajewski, P. (2017). Assessing change in a high-value landscape: Case study of the municipality of Sobotka, Poland. *Pol. J. Environ. Stud.* 26, 2603–2610. [CrossRef]
- [27]. Krajewski, P.; Solecka, I.; Cetera, B.M. (2017). Landscape Change Index as a Tool for Spatial Analysis. *IOP Conf. Ser. Mater. Sci. Eng.* 245, 072014. [CrossRef]
- [28]. Ku, D.N.; Sandeep, N.; Jyothi, S.; Madhu, T. (2017). Significant changes on land use/land cover by using remote sensing and GIS analysis-review. *Int. J. Eng. Sci. Comput.* 7, 5433– 5435.
- [29]. Kuldeep. T and Kamlesh, K (2011). Land Use / Land cover change detection in Doon valley (Dehradun Tehsil), Uttarakhand: using GIS & Remote Sensing Technique. *International Journal of Geomatics and Geosciences.* V.2, No 1.
- [30]. Li, X.; Zhang, X.; Yeh, A.; Liu, X. Parallel cellular automata for large-scale urban simulation using load-balancing techniques. *Int. J. Geogr. Inf. Sci.* 2010, 24, 803–820. [CrossRef]
- [31]. Li, X.; Zhou, Y.; Asrar, G.R.; Imhoff, M.; Li, X. (2017). The surface urban heat island response to urban expansion: A panel analysis for the conterminous United States. *Sci. Total Environ.* 605–606, 426–435. [CrossRef]
- [32]. Manonmani, R. and G.M.D. Suganya, (2010). Remote sensing and GIS application in change detection study in the urban zone using multi-temporal satellite. *Int. J. Geomat. Geosci.*, 1: 60–65.

- [33]. Mirzaei, P.A. (2015). Recent challenges in modeling of urban heat island. *Sustain. Cities Soc.* 19, 200–206. [CrossRef]
- [34]. Nowak, A.; Szamrej, J.; Latané, B. (1990). From private attitude to public opinion: A dynamic theory of social impact. *Psychol. Rev.* 97, 362–376. [CrossRef]
- [35]. Pal, S.; Ziaul, S. (2017). Detection of land use and land cover change and land surface temperature in English Bazar urban centre. *Egypt. J. Remote Sens. Space Sci.* 20, 125–145. [CrossRef]
- [36]. Portugali, J. *Complexity, Cognition and the City*; Springer: New York, NY, USA, 2011.
- [37]. Ranagalage, M.; Dissanayake, D.; Murayama, Y.; Zhang, X.; Estoque, R.C.; Perera, E.; Morimoto, T. (2018). Quantifying surface urban heat island formation in the world heritage tropical mountain city of Sri Lanka. *ISPRS Int. J. Geo-Inf.* 7, 341. [CrossRef]
- [38]. Ranagalage, M.; Estoque, R.C.; Handayani, H.; Zhang, X.; Morimoto, T.; Tadono, T.; Murayama, Y. (2018). Relation between urban volume and land surface temperature: A comparative study of planned and traditional cities in Japan. *Sustainability*, 10, 2366. [CrossRef]
- [39]. Ranagalage, M.; Estoque, R.; Murayama, Y. (2017). An urban heat island study of the Colombo metropolitan area, Sri Lanka, based on Landsat data (1997–2017). *ISPRS Int. J. Geo-Inf.*, 6, 189. [CrossRef]
- [40]. Rosa, A.; De Oliveira, F.S.; Gomes, A.; Gleriani, J.M.; Gonçalves, W.; Moreira, G.L.; Silva, F.G.; Ricardo, E.; Branco, F.; Moura, M.M.; et al. (2017). Spatial and temporal distribution of urban heat islands. *Sci. Total Environ.* 605–606, 946–956.
- [41]. Saarloos, D.J.M.; Arentze, T.A.; Borgers, A.W.J.; Timmermans, H.J.P. (2008). A multi-agent paradigm as structuring principle for planning support systems. *Comput. Environ. Urban Syst.* 32, 29–40. [CrossRef]
- [42]. Sharma, R.; Chakraborty, A.; Joshi, P. (2015). Geospatial quantification and analysis of environmental changes in urbanizing city of Kolkata (India). *Environ. Monit. Assess.*, 187, 4206. [CrossRef]
- [43]. Sexton, J.O.; Urban, D.L.; Donohue, M.J.; Song, C. (2013). Long-term land cover dynamics by multi-temporal classification across the Landsat-5 record. *Remote Sens. Environ.*, 128, 246–258. [CrossRef]
- [44]. Singh, P.; Kikon, N.; Verma, P. (2017). Impact of land use change and urbanization on urban heat island in Lucknow city, Central India: A remote sensing based estimate. *Sustain. Cities Soc.*, 32, 100–114. [CrossRef]
- [45]. Sultana, S.; Satyanarayana, A.N.V. (2018). Urban heat island intensity during winter over metropolitan cities of India using remote-sensing techniques: Impact of urbanization. *Int. J. Remote Sens.* 39, 6692–6730. [CrossRef]
- [46]. Swan, M. *Sensor M.* (2012). *The Internet of Things, Wearable Computing, Objective Metrics, and the Quantified Self 2.0*. *J. Sens. Actuator Netw.* 2012, 1, 217–253. [CrossRef]
- [47]. Tan, R.; Liu, Y.; Zhou, K.; Liao, L.; Tang, W. (2015) A game-theory based agent-cellular model for use in urban growth simulation: A case study of the rapidly urbanizing Wuhan area of central China. *Comput. Environ. Urban Syst.* 49, 15–29. [CrossRef]
- [48]. The World's Cities in 2016. T. W. C. in 2016—D. B. (ST/ESA/S.A.), Population Department, Department of Economic and Social Affairs, United Nations. 2016. Available online: http://www.un.org/en/development/desa/population/publications/pdf/urbanization/the_worlds_cities_in_2016_data_booklet.pdf (accessed on 28 August 2018).
- [49]. Wang, R.; Dourdour, A.; Murayama, Y. (2018). Spatiotemporal simulation of future land use/cover change scenarios in the Tokyo metropolitan area. *Sustainability*, 10, 2056. [CrossRef]
- [50]. Weng, Q.; Lu, D.; Schubring, J. (2004). Estimation of land surface temperature-vegetation abundance relationship for urban heat island studies. *Remote Sens. Environ.*, 89, 467–483. [CrossRef]
- [51]. Wilkie, D.S., and Finn, J.T. (1996). *Remote Sensing Imagery for Natural Resources Monitoring*. Columbia University Press, New York. p. 295.
- [52]. Wooldridge, M. *An Introduction to Multiagent Systems*; John Wiley & Sons: Hoboken, NJ, USA, 2009. Portugali, J. *Complexity, Cognition and the City*; Springer: New York, NY, USA, 2011.
- [53]. Zhang, Q., and J. Wang, (2003). “A Rule-based Urban Land Use Inferring Method for Fineresolution Multispectral Imagery,” *Canadian Journal of Remote Sensing*, 29(1):1–13.
- [54]. Zhang, Y. *CityMatrix—An Urban Decision Support System Augmented by Artificial Intelligence*. Master's Thesis, Massachusetts Institute of Technology, Cambridge MA, USA, 23 October 2017. Available online: <https://dam-prod.media.mit.edu/x/2017/08/23/ryanz-ms-17.pdf> (accessed on 5 May 2019).

Aminu Abdulwahab, et. al. “Heat Temperature Effect on Land-use and Land-cover Dynamics using Geospatial Techniques from Normalize Build-up Index (NDBI), Land Surface Temperature (LST) and Normalize Vegetation Index (NDVI).” *IOSR Journal of Environmental Science, Toxicology and Food Technology (IOSR-JESTFT)*, 14(7), (2021): pp 16-37.